Newton's descent method for the determination of invariant tori

Y. Lan,[1] C. Chandre,[2] and P. Cvitanović[1]
[1]*Center for Nonlinear Science, School of Physics, Georgia Institute of Technology, Atlanta, Georgia 30332-0430, USA*
[2]*Centre de Physique Théorique, Luminy, Case 907, F-13288 Marseille cedex 09, France*
(Received 26 August 2005; revised manuscript received 6 February 2006; published 6 October 2006)

We formulate a fictitious-time-flow equation which drives an initial guess torus to a torus invariant under a given dynamics, provided such a torus exists. The method is general and applies in principle to continuous time flows and discrete time maps in arbitrary dimension and to both Hamiltonian and dissipative systems.

DOI: 10.1103/PhysRevE.74.046206 PACS number(s): 05.45.−a, 45.10.Db, 45.50.Pk, 47.11.−j

I. INTRODUCTION

Analysis of dynamical systems in terms of invariant phase-space structures provides important insights into the behavior of physical systems. The simplest such invariants are equilibria, points in phase space which are stationary solutions or zero-dimensional invariants of the flow. They and their stable and unstable manifolds yield information about the topology of the flow. The role played by the next class of flow invariants, periodic orbits, in the topological organization of phase space and the computation of long-time dynamical averages is well known (for an overview, see Ref. [1]). A periodic orbit is topologically a circle or an invariant one-torus for a flow, and a set of discrete points or an invariant zero-torus for a map, embedded in a d-dimensional phase space. Higher-dimensional invariant tori also frequently play an important role in the dynamics; we refer the reader to Ref. [2] for further references to the literature. Invariant tori of dimension lower than the dimension of the dynamical flow can be normally hyperbolic and thus stay discrete [3,4]. In Hamiltonian systems, Kolmogorov-Arnold-Moser (KAM) theory implies that invariant tori occur in Cantor sets, and such tori play key roles in the phase-space transport [5,6]. For two-degree-of-freedom Hamiltonian flows (i.e., four-dimensional phase space), two-dimensional invariant tori act as barriers to diffusion across phase space, and for higher-dimensional flows similar structures are effectively hindering the orbit diffusion (Arnold diffusion). The breakup of these structures leads to qualitative changes in phase-space dynamics. In dissipative systems like Newtonian fluids, quasiperiodic motion on two- or higher-dimensional tori is one of the fundamental routes to the eventual turbulent motion [7,8].

Many methods for determining periodic orbits exist in the literature [1,9,10]. The lack of comparably effective methods for the determination of higher-dimensional invariant structures including invariant tori has stymied the exploration of the phase spaces of high-dimensional flows, a focus of much recent research [2,11]. In this paper, we concentrate on the algorithms for the numerical computation of invariant tori in both Hamiltonian and dissipative systems.

Signal processing methods like frequency analysis [12,13], based on the analysis of trajectories, can detect elliptic invariant tori since these tori influence the behavior of nearby trajectories in a persistent way. Bailout methods [14,15] effectively locate the elliptic regions in a nonintegrable system by embedding the dynamical system into a larger phase space. Reference [16] describes a variational technique designed to find regular orbits in a phase space with mixed dynamics. However, these methods can only detect trajectories with nonpositive Lyapunov exponents. They single out regular motions in a phase space but can not exactly determine a torus unless it is stable. Due to their relative ease of identification, in special cases, periodic orbits are used to study invariant tori and their breakups. For example, in the Greene's criterion approach [17–19] one studies a sequence of periodic orbits which converges to a given invariant torus. Such approaches have been mainly applied to the determination of tori of Hamiltonian systems with two degrees of freedom.

Other techniques to determine invariant tori are specific to the phase-space dynamics of the system under consideration, most often a Hamiltonian system. Early attempts like the spectral balance method were based on computation of quasiperiodic orbits [20,21], the closure of which constitutes the invariant torus. To overcome the small divisor problems associated with the flow on a torus, recent research employed a geometric point of view and focused on the invariant torus itself. Efforts are devoted to find the solution of the so-called invariance condition which ensures the invariance of a parametrized object in phase space. Invariance conditions are functional equations for maps [22–27] and first-order partial differential equations (PDE's) for flows [28–30]. These equations can be solved by Newton's method or the Hadamard graph transform technique [4]. In view of the periodicity in the angle variables, Fourier transforms are widely used in the computation [31–37]. For Hamiltonian systems, the action principle and the Hamilton-Jacobi equation are also frequently used in the calculation of periodic and quasiperiodic orbits [32,38–42].

In this paper, we use a particular invariance condition to derive a PDE which evolves a guess torus to an invariant one for flows and maps embedded in d-dimensional phase spaces. The method is a generalization of the differential "Newton descent" method originally developed to locate periodic orbits of flows [46,47], which can be viewed as a variant of the multishooting method in boundary value problems [43–45]. When the representative points on the guess torus achieve a near-continuous distribution, a PDE is derived which governs their evolution to a true invariant torus. In spirit, this is similar to the approach used in Ref. [32] and thus high accuracy is expected. However, our method is stable and thus applies to more general systems, including

searches for partially hyperbolic tori embedded in chaotic regions of a phase space. In a general dynamical system, the phase-space structure can be extremely complex and the global stability of our algorithm is of key importance for the convergence of the searching program. In our numerical computation, an adaptive scheme is used which keeps changing the step size according to the smoothness of the evolution. In addition to the adaptive step size, we further speed up our searches by utilizing the continuity of the evolution PDE. These salient features will be explained in detail in what follows.

In Sec. II we derive the Newton descent equation which governs the fictitious time dynamics. The numerical implemention of this equation is discussed in Sec. III. The method is further illustrated in Sec. IV through its application to the determination of one-tori of the standard map, of two-tori of a forced pendulum flow (three-dimensional phase space), of one- and two-tori of two coupled standard maps (a four-dimensional symplectic map), and of two-tori of the Kuramoto-Sivashinsky system (infinite-dimensional phase space). In particular, we provide evidence that the method converges up to the threshold of existence of a given invariant torus and yields estimates of the critical thresholds of the breakup of invariant tori of two-degree-of-freedom Hamiltonian systems.

II. NEWTON DESCENT METHOD FOR INVARIANT TORI

We start by deriving a fictitious time evolution equation for the determination of a one-dimensional (1D) invariant torus of a d-dimensional map $\mathbf{f}:\mathbb{R}^d\to\mathbb{R}^d$. The method can be extended to the determination of invariant m-tori of d-dimensional maps and flows. We stress here that the maps or flows and the invariant tori are assumed to be sufficiently smooth in the following.

A fixed point (zero-dimensional invariant torus) $\mathbf{x}=\mathbf{f}(\mathbf{x})$ is a point which is mapped onto itself under the action of $\mathbf{f}$. Likewise, a one-dimensional invariant torus of $\mathbf{f}$ is a loop in $\mathbb{R}^d$ which is mapped onto itself under the action of $\mathbf{f}$. If points on the invariant one-torus are parametrized by a cyclic variable $s\in[0,2\pi]$, with $\mathbf{x}(s)=\mathbf{x}(s+2\pi)$, a point $\mathbf{x}(s)$ is mapped into another point on the invariant torus

$$\mathbf{f}(\mathbf{x}(s))=\mathbf{x}(s+\omega(s)), \tag{1}$$

where $\omega(s)$ is the local parametrization s-dependent shift. In other words, the full phase space dynamics $\mathbf{f}$ induces a one-dimensional circle map on the invariant one-torus:

$$s\mapsto s+\omega(s) \mod 2\pi. \tag{2}$$

We also parametrize our *guess* for the invariant one-torus, the loop $\mathbf{x}(s,\tau)$, by $s\in[0,2\pi]$, with $\mathbf{x}(s,\tau)=\mathbf{x}(s+2\pi,\tau)$. Together with the "fictitious time" τ, to be defined below, this parametrizes a continuous family of guess loops, with the initial one at the beginning ($\tau=0$) and the truly invariant one at the end ($\tau=\infty$). However, for an arbitrary loop there is no unique definition of the shift ω, as the loop is not mapped onto itself under the action of $\mathbf{f}$. Intuitively, ω should be determined by requiring that the d-dimensional distance vector between the circle map image of a point on the loop at s and the corresponding point on the iterate of the loop,

$$\mathbf{F}(s,\tau)=\mathbf{x}(s+\omega(s,\tau),\tau)-\mathbf{f}(\mathbf{x}(s,\tau)), \tag{3}$$

be minimized. For example, if the guess loop is sufficiently close to the desired invariant one-torus, $\omega(s,\tau)$ can be fixed by intersecting the loop with a hyperplane normal to the loop and cutting through the image of loop $\mathbf{f}(\mathbf{x}(s,\tau))$.

In this exploratory foray into the world of compact higher-dimensional invariant manifolds we shall make the simplest choice at each turn. In particular, we are free to choose any parametrization s which preserves ordering of points along the invariant one-torus—i.e., any circle map (2) that is strictly monotone, $1+d\omega/ds>0$. For an irrational rotation number a strictly monotone circle map can be conjugated to a constant shift, so in what follows we *define* the s parametrization dynamically by requiring that the action of the dynamics $\mathbf{f}$ on both the guess loop and the target invariant one-torus be a rotation with constant (in s but not in τ) shift ω,

$$s\mapsto s+\omega \mod 2\pi. \tag{4}$$

The invariance condition (1) with conjugate dynamics (4) has been used previously in the literature [33,34]. We now design a stable scheme which yields a parametrization $\mathbf{x}(s)$ satisfying Eq. (1) together with Eq. (4).

Following the approach of Refs. [46,47] originally developed to locate periodic orbits of flows, we now introduce the simplest cost functional that measures the average distance squared, Eq. (3), of the guess loop from its iterate:

$$\mathcal{F}^2[\tau]=\oint\frac{ds}{2\pi}\mathbf{F}(s,\tau)^2. \tag{5}$$

A similar functional was used in the stochastic path extremization [48]. Here $\mathcal{F}^2[\tau]=\mathcal{F}^2[\mathbf{x},\omega]$ is a functional, as it depends on the infinity of the points $\mathbf{x}(s,\tau)$ that constitute the loop for a given τ. If the loop is an invariant one-torus conjugate to rotation by ω, $\mathcal{F}^2=0$; otherwise, $\mathcal{F}^2>0$. At fictitious time τ we compute the cost due to the two mappings: one is the iterate $\mathbf{f}(\mathbf{x}(s,\tau))$ of the loop, and the other the circle map $s\mapsto s+\omega(\tau)$ along the loop. The fictitious time evolution should monotonically decrease the distance between a loop and its iterate, as measured by the functional $\mathcal{F}^2[\tau]$, by moving both the totality of loop points $\mathbf{x}(s,\tau)$ and modifying the shift $\omega(\tau)$.

With constant shift circle map (4) the variation of $\mathcal{F}^2[\tau]$ under the (yet unspecified) fictitious time variation $d\tau$ is

$$\frac{d}{d\tau}\mathcal{F}^2[\tau]=2\oint\frac{ds}{2\pi}\left(\mathbf{F}(s,\tau)\cdot\frac{d\mathbf{F}}{d\tau}(s,\tau)\right), \tag{6}$$

where

$$\frac{d}{d\tau}\mathbf{F}(s,\tau)=\frac{\partial\mathbf{x}}{\partial\tau}(s+\omega(\tau),\tau)+\mathbf{v}(s+\omega(\tau),\tau)\frac{d\omega(\tau)}{d\tau}$$

$$-J(\mathbf{x}(s,\tau))\frac{\partial\mathbf{x}}{\partial\tau}(s,\tau),$$

$$\mathbf{v}(s,\tau) = \frac{\partial \mathbf{x}}{\partial s}(s,\tau).$$

The adjustment in the loop tangent direction $\mathbf{v}$ is needed to redistribute points along the loop in order to ensure a constant shift parametrization s, and the $[d \times d]$ Jacobian matrix of the map $J = \partial \mathbf{f}/\partial \mathbf{x}$ moves the loop point $\mathbf{x}(s,\tau)$ in the "Newton descent" direction.

Again we design a fictitious time flow in the space of loops by taking the simplest choice, in the spirit of the Newton method [47],

$$\frac{d\mathbf{F}}{d\tau} = -\mathbf{F}, \tag{7}$$

for which $\mathcal{F}^2[\mathbf{x},\omega]$ decreases exponentially with fictitious time τ:

$$\mathcal{F}^2[\tau] = \mathcal{F}^2[0]e^{-2\tau}. \tag{8}$$

Written out in detail, the Newton descent equation for a guess loop,

$$\frac{\partial \mathbf{x}}{\partial \tau}(s+\omega,\tau) + \frac{\partial \mathbf{x}}{\partial s}(s+\omega,\tau)\frac{\partial \omega}{\partial \tau}(\tau) - J(\mathbf{x}(s,\tau))\frac{\partial \mathbf{x}}{\partial \tau}(s,\tau) = \mathbf{f}(\mathbf{x}(s,\tau)) - \mathbf{x}(s+\omega,\tau), \tag{9}$$

evolves points $\mathbf{x}(s,0)$ on the $\tau=0$ initial guess loop to the points $\mathbf{x}(s)=\mathbf{x}(s,\infty)$, $s \mapsto s+\omega$, $\omega=\omega(s,\infty)$, on the target one-torus, provided that the τ flow does not get trapped in a local minimum with $\mathcal{F}^2[\infty]>0$. For a bad initial guess the Newton method for determining the roots of a one-dimensional function can fail by getting trapped by a critical point of the function. The same applies to the Newton descent equation (7) where in our numerical searches we sometimes observe trapping by points with critical directions. In such cases, "τ" in Eq. (8) cannot go to infinity, and we restart the search with a new initial guess torus. A good initial guess for the target torus should lie in its basin of attraction under the fictitious dynamics. As the search takes place in a high-dimensional discretized-loop space, we have very limited intuition as to the form of these basins of attraction. The "Newton descent" PDE (9) which governs evolution of the loop points in fictitious time τ and along loop direction s is the main result of this paper, which bears a close similarity to the PDE for the homotopy evolution of pseudoholomorphic curves [49,50].

The choice of the minimization scheme (7) is not arbitrary but can be derived in a more physical way through a similar multishooting argument discussed in Ref. [47]. We present here a derivation with the calculus of variations for simplicity [46]. It is important to notice that Eq. (7) is not a gradient descent equation for blindly minimizing the functional $\mathcal{F}^2$ since the direction given by its right-hand side is not along the gradient of $\mathcal{F}^2$ or $\mathbf{F}^2$. A similar argument has been used in the derivation of a globally convergent modified Newton's method in Ref. [45]. Equation (9) is an infinitesimal variant of Newton's method. The cost functional (5) is used to show the monotonous decrease of the discrepancy between the guess and the true torus.

Generalization to searches for invariant m-tori is immediate: the guess m-torus is parametrized by $\mathbf{s}=(s_1,s_2,\ldots,s_m) \in [0,2\pi]^m$, periodic in each cyclic coordinate,

$$\mathbf{x}(\mathbf{s}+2\pi\mathbf{k}) = \mathbf{x}(\mathbf{s}) \quad \text{for all } \mathbf{k} \in \mathbb{Z}^m, \tag{10}$$

with m incommensurate shifts $\boldsymbol{\omega}=(\omega_1,\omega_2,\ldots,\omega_m)$ [51]. Now the fictitious time flow (9) has an $[d \times m]$ velocity tensor $\mathbf{v}$ which spans the m-dimensional tangent space of the guess torus embedded in a d-dimensional phase space. Furthermore, the fictitious time flow searches (9) for invariant tori can also be adopted to smooth continuous time flows by reducing the flow to a Poincaré return map on any local Poincaré section which intersects transversally the trajectories in the neighborhood of the guess $(m+1)$-torus. We will provide examples in what follows.

In general, each independent tangent vector of an invariant m-torus transformation along a given cyclic parameter s_k has a unit eigenvalue, leaving arbitrary the phase of the parametrization. We need to impose further constraints to get rid of this arbitrariness. For example, for the Jacobian matrix of a continuous time periodic orbit (a one-torus) the velocity vector is an eigenvector with a unit eigenvalue and Newton descent equations need to be supplemented with a constraint (a Poincaré section) in order to determine the orbit together with its period. On the other hand, if the flow is Hamiltonian and the invariant m-torus is located on a fixed energy surface $H(\mathbf{p},\mathbf{q})=E$, the constraint $dH/d\tau=0$ is needed to ensure the conservation of the energy by the fictitious time dynamics.

In the case at hand, there are two alternative ways to impose the constraint: We may or may not fix ω *a priori*.

(a) If we are searching for an invariant one-torus of a fixed shift ω, the fictitious time flow should not change the shift along the loop,

$$d\omega/d\tau = 0. \tag{11}$$

(b) If we are searching for an invariant one-torus of a given topology or on a specific energy surface, the shift $\omega=\omega(\tau)$ varies with the fictitious time τ and is to be determined simultaneously with the one-torus itself. In this case we impose the *phase condition* [30]

$$\oint ds \left(\mathbf{v}(s,\tau) \cdot \frac{\partial \mathbf{x}}{\partial \tau}(s,\tau) \right) = 0, \tag{12}$$

which ensures that during the fictitious time evolution the average motion of the points along the loop equals zero. Empirically, for this global loop constraint the fictitious time dynamics is more stable than for a single-point constraint such as $\delta\mathbf{x}(0,\tau)=0$. For an m-torus, $\mathbf{v}(s,\tau)$ is a $[d \times m]$ tensor and Eq. (12) yields m constraints. For energy-conserving Hamiltonian systems, one phase condition has to be replaced by the energy conservation condition

$$\frac{1}{2\pi}\oint ds\, \boldsymbol{\nabla} H(\mathbf{x}(s,\tau)) \cdot \frac{\partial \mathbf{x}(s,\tau)}{\partial \tau} = E - \frac{1}{2\pi} ds \oint H(\mathbf{x}(s,\tau)), \tag{13}$$

where a fixed E fixes the energy shell under consideration.

The two cases are analogous to continuous time Hamiltonian flow periodic orbit constraints: case (a) corresponds to fixing the period and varying the energy shell and case (b) to fixing the energy and computing the period of a periodic orbit of a given topology.

The examples of Secs. IV A–IV C illustrate the constant shift ω constraint (11); the examples of Fig. 4and Sec. IV D illustrate the phase condition (12).

III. NUMERICAL IMPLEMENTATION

Due to the periodic boundary condition (4), it is convenient to expand the loop point $\mathbf{x}$, the Jacobian matrix J, the map $\mathbf{f}$, and the loop tangent $\mathbf{v}$ as a discrete Fourier series

$$\mathbf{x}(s,\tau) = \sum_k \mathbf{a}_k(\tau) e^{iks},$$

$$J(\mathbf{x}(s,\tau)) = \sum_k J_k(\tau) e^{iks},$$

$$\mathbf{f}(\mathbf{x}(s,\tau)) = \sum_k \mathbf{b}_k(\tau) e^{iks},$$

$$\mathbf{v}(s,\tau) = i\sum_k k\mathbf{a}_k(\tau) e^{iks} \tag{14}$$

[$\mathbf{a}_k^* = \mathbf{a}_{-k}$ due to the reality of $\mathbf{x}(s,\tau)$, and similar relations hold for J_k and $\mathbf{b}_k$], and rewrite the Newton descent PDE (9) as an infinite ladder of ordinary differential equations:

$$\left(\frac{d\mathbf{a}_k}{d\tau} + ik\mathbf{a}_k\frac{d\omega}{d\tau}\right)e^{ik\omega} - \sum_l J_{k-l}\frac{d\mathbf{a}_l}{d\tau} = \mathbf{b}_k - \mathbf{a}_k e^{ik\omega}. \tag{15}$$

Finally, the unit stability eigenvalue along the loop tangent direction $\mathbf{v}(s,\tau)$ needs to be eliminated by adding to Eq. (15) either the constant shift ω constraint (11) or the phase condition (12). In the Fourier representation the phase condition is given by

$$\sum_k k\mathbf{a}_k^* \cdot \partial\mathbf{a}_k/\partial\tau = 0. \tag{16}$$

If the target torus is smooth and has a well-behaved Fourier representation, the monotone decrease with τ of the functional $\mathcal{F}^2$, given by Eq. (6), guarantees that the solution of Eq. (15) approaches a fixed point which, provided that $\mathcal{F}^2 = 0$, is the Fourier representation of the target invariant torus. For tori with less regularity, the correct convergence is not assured [52].

In our numerical calculations, we represent the loop by a discrete set of points $\{\mathbf{x}(s_1),\ldots,\mathbf{x}(s_{2N})\}$. The search is initialized by a $2N$-point guess torus. The Fourier transforms of $\mathbf{x}$, $\mathbf{v}$, and J are computed numerically, yielding M complex Fourier coefficients $\mathbf{a}_k$, $\mathbf{b}_k$, and J_k, respectively. To maintain numerical accuracy, we choose $M \leqslant N$ and set $\mathbf{a}_k = 0$, $\mathbf{b}_k = 0$, and $J_k = 0$ for $|k| \geqslant M$. We terminate the numerical integration of the fictitious time dynamics (19) when the distance (3) falls bellow a specified cutoff. In the Fourier representation, we stop when distance reaches the *termination value* Δ defined as

$$\max_k \|\mathbf{F}_k\| = \max_{k,j} |b_{k,j} - a_{k,j}e^{ik\omega}| < \Delta, \tag{17}$$

where $a_{k,j}$ and $b_{k,j}$ denote the jth component of $\mathbf{a}_k$ and $\mathbf{b}_k$.

While the algorithm is more efficient with a good initial guess, in practice it often works for rather inaccurate initial guesses. If the initial guess is bad or the target invariant torus does not exist, the evolution diverges. Then another search is initiated, with a new guess. This guess torus can either be derived from the integrable limit, like the examples of Secs. IV A–IV C, or from numerical exploration, like the example of Sec. IV D. If the invariant torus is isolated or partially hyperbolic, far away from the integrable limit, it can be a challenging problem to initialize the search for an embedded invariant torus. However, once provided with a reasonable guess, our method is able to reliably locate the torus with relatively high accuracy.

Since the invariant torus corresponds to a stationary set of equations (9) explored ergodically by long-time dynamics, the accuracy of the fictitious time steps is not important as long as the successive tori remain in the domain of attraction of the desired invariant torus. A simple Euler step integration method suffices for our purposes. If we try to find a high-order torus (large m) in a high-dimensional phase space (large d) with M complex Fourier modes, we have to solve a $[(2M)^m d+m]$-dimensional linear system

$$\mathcal{M}\begin{pmatrix} d\mathbf{a}_k/d\tau \\ d\omega/d\tau \end{pmatrix} = \begin{pmatrix} \mathbf{F}_k \\ 0 \end{pmatrix}, \quad \text{with } \mathbf{F}_k = \mathbf{b}_k - \mathbf{a}_k e^{ik\omega},$$

derived from Eq. (15) with the constraint (11) or (16), for $(2M)^m d$ $d\mathbf{a}_k/d\tau$'s and m $d\omega/d\tau$'s in each time step. This involves inverting the large $\{[(2M)^m d+m]\times[(2M)^m d+m]\}$ matrix $\mathcal{M}$ repeatedly during the integration which may constitute a major bottleneck in such calculations. In our numerical implementation, the matrix inversion by the LU decomposition [45] consumes most of the computational time. We employ a speed-up scheme, based on the continuity of the evolution of Eq. (15). Once we have the LU decomposition of $\mathcal{M}$ at one step, we use it to approximately invert the new $\mathcal{M}$ matrix in the next step, with accurate inversion achieved by iterative approximate inversion [45]. In practice, we find that one LU decomposition can be used for many $\delta\tau$ evolution steps. The more steps in which we used the same LU decomposition, the more iterations at each step are needed to get the accurate inversion. After the number of such iterations exceeds some fixed given maximum number, another LU decomposition is performed. The number of integration steps following one decomposition is an indication of the smoothness of the evolution, and we further accelerate our program by adjusting accordingly the step size $\delta\tau$: the greater the number, the bigger the step size. Near the final stage of convergence, the evolution becomes so smooth that the step size can be brought all the way up to $\delta\tau = 1$, recovering the full undamped Newton-Raphson step and acquiring the desired quadratic convergence.

IV. EXAMPLES

We now test the Newton descent method for determining invariant tori on a series of systems of increasing dimension-

ality: a two-dimensional area-preserving standard map, a Hamiltonian flow with one and half degrees of freedom (a forced pendulum), a four-dimensional symplectic map (two coupled standard maps), and a dissipative PDE (the Kuramoto-Sivashinsky system). In the following, the representative points are uniformly distributed on the initial guess torus.

A. Critical tori of the standard map

As our first example we search for invariant one-tori of a two-dimensional area-preserving map, the standard map

$$q_{n+1} = q_n + p_{n+1} \mod 2\pi,$$

$$p_{n+1} = p_n + K \sin q_n, \tag{18}$$

where K is the nonlinearity parameter. For $K=0$ the map is a constant rotation in q, and for $K>0$ its phase space is a mixture of KAM tori and chaotic regions. In the Fourier space the initial guess loop $\mathbf{x}=(q,p)$ and its image $\mathbf{f}(\mathbf{x})=(q+p+K\sin q, p+K\sin q)$ are expanded as

$$\mathbf{x}(s,\tau) = \mathbf{s} + \sum_k \mathbf{a}_k(\tau) e^{iks}, \quad \mathbf{s} = (s,0),$$

$$\mathbf{f}(\mathbf{x}(s,\tau)) = \mathbf{s} + \sum_k \mathbf{b}_k(\tau) e^{iks}.$$

The linear term $\mathbf{s}$ in Eq. (15) is needed to compensate the modulus 2π operation on q in Eq. (18). Substitution into Eq. (9) yields

$$\left(\frac{d\mathbf{a}_k}{d\tau} + ik\mathbf{a}_k\frac{d\omega}{d\tau}\right)e^{ik\omega} + \delta_{0k}\frac{d\omega}{d\tau}\mathbf{e}_1 - \sum_l J_{k-l}\frac{d\mathbf{a}_l}{d\tau}$$
$$= \mathbf{b}_k - \mathbf{a}_k e^{ik\omega} - \delta_{0k}\omega\mathbf{e}_1, \tag{19}$$

where $\mathbf{e}_1=(1,0)$. If we denote by $\mathbf{F}_k$ the distance (3) on the right hand side of Eq. (19), the invariant torus condition for constant shift (11) is $\mathbf{F}_{k=0}$ for all k—i.e., $\mathbf{b}_k=\mathbf{a}_k e^{ik\omega}$ for $k\neq 0$ and $\mathbf{b}_0=\mathbf{a}_0+\omega\mathbf{e}_1$.

As the first test of our searching method, we apply it to the determination of the golden-mean invariant torus, with the shift fixed to $\omega_g=2\pi(\sqrt{5}-1)/2$ and the fixed shift constraint (11). We use as the initial guess for the fictitious time dynamics the invariant torus of the linear standard map with $K=0$ and the golden-mean shift $\mathbf{x}(s,0)=(s,\omega_g)$, represented by the straight line in Fig. 1. In order to test that the method works for a smooth invariant torus we set $K=0.5$ and integrate the fictitious time dynamics (19) with $2N=256$ point discretization of the torus, $M=64$ complex Fourier mode truncation, and $\Delta=2\times10^{-6}$ termination value (17). The resulting invariant torus is shown by the dotted line in Fig. 1.

Next, we apply the method to a sequence of golden-mean invariant tori with increasing K. Numerics indicates that there exists a critical value $\tilde{K}_c$ such that when $K<\tilde{K}_c$, the fictitious time dynamics converges exponentially, as in Eq. (8), but for $K>\tilde{K}_c$, it diverges. The critical value $\tilde{K}_c$ depends sensitively on the torus discretization $2N$ and the termination

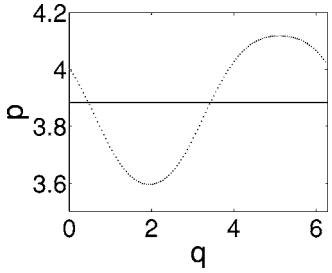

FIG. 1. The $\omega=\omega_g=3.883\ldots$ golden-mean invariant torus of the standard map (18) for $K=0.5$; the straight line represents the initial condition.

value Δ. $\tilde{K}_c(N)$ computed for $\Delta=2\times10^{-6}$ and several values of N is

$2N$	64	128	256	512	1024
$\tilde{K}_c(N)$	0.34	0.80	0.93	0.9656	0.9762

The golden-mean critical invariant torus is depicted in Fig. 2(a) for $2N=1024$ points discretization of the torus. Small oscillating structures in the critical torus whose resolution would require higher-frequency Fourier components are already visible. The uneven distribution of representative points [s parametrization's embedding into the (q,p) plane] along the torus indicates the drastically varying stretching rate on the invariant torus close to the breakup [53,54]. Our

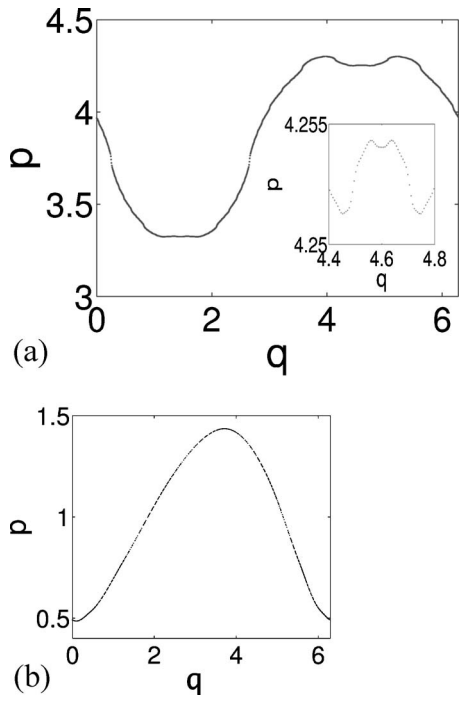

FIG. 2. Invariant tori for the standard map (18) for (a) $\omega=\omega_g$ at $K=\tilde{K}_c(512)=0.9762$ close to the golden-mean torus critical value K_c, termination value $\Delta=2\times10^{-6}$. The inset, which is an enlargement of the curve around $q=4.6$, illustrates the fine structure of the nearly critical torus. (b) Irrational shift $\omega=2\pi(\pi-3)$ at the estimated critical value $\tilde{K}_c(512)=0.4313$, termination value $\Delta=4\times10^{-6}$. $2N=1024$ torus point discretization.

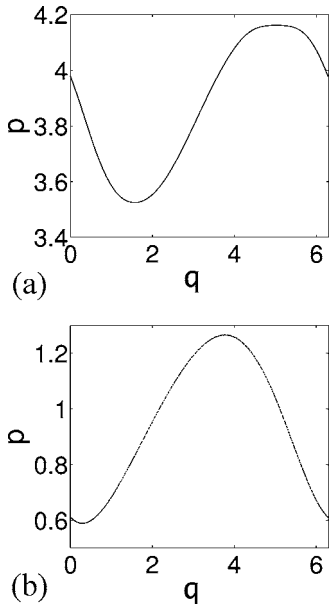

FIG. 3. The invariant tori for the standard map (18) with smaller termination values Δ than in Fig. 2, the same number of torus points, $2N=1024$: (a) $\omega=\omega_g$ with $\tilde{K}_c=0.6188$ and $\Delta=10^{-6}$ and (b) $\omega=2\pi(\pi-3)$ with $\tilde{K}_c=0.3004$ and $\Delta=2\times10^{-6}$.

numerical estimate of the critical K_c parameter is in agreement with Greene's estimate [17] that the golden-mean invariant torus breaks up at the critical value $K_c\approx0.9716$. Moreover, we find that for large values of the $2N$-point discretization of the torus, $\tilde{K}_c(N)$ approaches K_c approximately as N^{-1}.

As the Newton descent method does not depend on the specific arithmetical properties of the invariant torus shift, it should work for arbitrary irrational shifts. As an example, we study the family of invariant tori with shift $\omega=2\pi(\pi-3)$. We found that the critical value of convergence $\tilde{K}_c\approx0.4313$ for $2N=1024$ and $\Delta=4\times10^{-6}$. The critical torus, depicted in Fig. 2(b), exhibits nonuniform s-parametrization and oscillating structure, though much less so than the golden-mean critical torus.

In order to assess the sensitivity of the method to the choice of the termination value Δ, we have studied its influence on the estimation of the critical $\tilde{K}_c$. For the golden-mean example, a decrease in the termination value to $\Delta=10^{-6}$ for $\omega=\omega_g$ and $2N=1024$ point discretization of the torus yields $\tilde{K}_c=0.6188$, which is much smaller than the value of $\tilde{K}_c=0.9762$ obtained for $\Delta=2\times10^{-6}$. The corresponding invariant torus for $\Delta=10^{-6}$ is depicted in Fig. 3(a). We notice that this torus looks much smoother than the one obtained for $\Delta=2\times10^{-6}$ [see Fig. 2(a)]. Similarly, for $\omega=2\pi(\pi-3)$ a decrease of the termination value to $\Delta=2\times10^{-6}$ yields also a smaller critical value $\tilde{K}_c=0.3004$. The corresponding invariant torus for $\Delta=2\times10^{-6}$ is shown in Fig. 3(b). The points are distributed more evenly than in Fig. 2(b), indicating that the invariant torus obtained using this termination value is far from criticality.

In summary: For fixed $2N$-point discretization of the torus, if Δ is too small, then $\tilde{K}_c(N)<K_c$, while if Δ is too large, then $\tilde{K}_c(N)>K_c$. At the threshold of criticality the invariant torus is fractal and thus cannot be resolved by a smooth finite Fourier truncation. The discrepancy between the invariant torus and its numerical discretization has a complicated influence on the fictitious time dynamics, not elucidated in this investigation. If Δ is too small, high oscillating modes in the critical torus preclude a numerical representation, which leads to an estimate of $\tilde{K}_c$ lower than the true K_c and renders the torus smoother. If Δ is too large, the discretization will average out the small oscillating features, converging to a grid beyond the critical value. With increasingly refined $2N$-point discretization of the torus, the value of Δ needs to be chosen carefully in order to improve the K_c estimate.

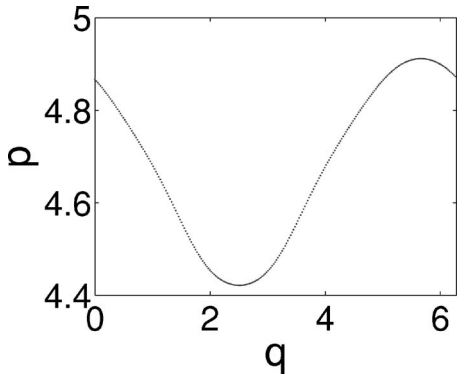

FIG. 4. An invariant torus of the standard map (18) for $K=0.352$ obtained by the fictitious time dynamics with the phase condition (12). The method yields a shift $\omega\approx4.67857$. $2N=256$ point discretization of the torus, termination value $\Delta=2\times10^{-6}$.

So far we have determined invariant tori of the standard map by imposing a constant shift condition (11). An alternative is the phase condition (12) which requires that the motion of representative points along the torus during the fictitious time dynamics average to zero. In this case the shift ω is not fixed, but is determined by the fictitious time dynamics. We test this condition by starting with an initial torus $\mathbf{x}(s)=(s,9\omega_g/10)$ discretized on $2N=256$ points, with termination value $\Delta=2\times10^{-6}$. For $K=0.352$ the Newton descent method yields the invariant torus of the standard map shown in Fig. 4, with shift $\omega\approx4.678\,57$. In general, the technique which varies the frequency of the torus might be useful. Very often in dissipative systems strong evidence shows that an isolated invariant torus exists in some region of the phase space with unknown shift. Our method can be used to determine both the torus and the shift simultaneously. One such an example is given in Sec. IV D.

B. Periodically forced Hamiltonian system

As our second test case, we consider the forced pendulum

$$H(p,x,t)=p^2/2-\varepsilon[\cos x+\cos(x-t)], \tag{20}$$

a time-dependent Hamiltonian flow with 1.5 degrees of freedom. $H(p,x,t)$ is a periodic function of the angle variable x and the time variable t, with dynamics on $\mathbb{R}\times\mathbb{T}^2$. The

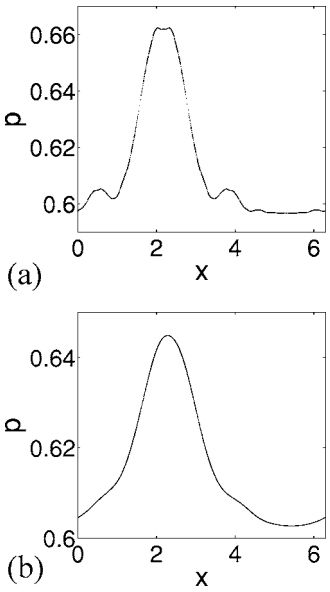

FIG. 5. Invariant tori of Hamiltonian (20) with $\omega=\bar{\omega}_g$ obtained by the fictitious time dynamics with $2N=1024$ and two different termination values: (a) $\Delta=2\times10^{-6}$ yields a critical value $\tilde{\varepsilon}_c=0.02781$, and (b) $\Delta=10^{-6}$ yields an underestimate $\tilde{\varepsilon}_c=0.01844$.

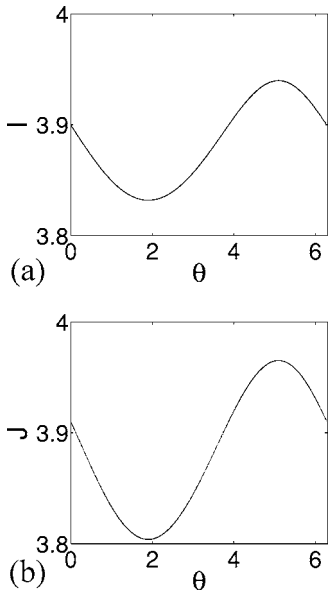

FIG. 6. A one-dimensional invariant torus with shift ω_g of Eq. (22) with $\epsilon_1=0.1$, $\epsilon_2=0.15$, and $\epsilon_3=0.005$: (a) I-θ projection and (b) J-θ projection. $2N=512$ point discretization of the torus, termination value $\Delta=10^{-6}$.

Poincaré return map for the stroboscopic section $t=0 \bmod 2\pi$ is a reversible area-preserving map. The Jacobian J required for the fictitious time dynamics (9) is evaluated by integrating

$$\dot{J}=AJ,\ A=\begin{pmatrix}0 & 1\\ -\epsilon[\cos x+\cos(x-t)] & 0\end{pmatrix},\quad J(0)=1. \tag{21}$$

We apply the fixed shift condition (11) Newton descent to the determination of the invariant torus with the golden-mean shift $\omega=\bar{\omega}_g=(\sqrt{5}-1)/2$. For the initial guess torus we take the golden-mean torus of Hamiltonian (20) with $\varepsilon=0$—i.e., $\mathbf{x}(s)=(s,\bar{\omega}_g)$. We define $\tilde{\varepsilon}_c(N)$ to be the minimum value of the parameter of the model at which the algorithm defining the fictitious time dynamics with $2N$ sampling points fails to converge at fixed Δ. The critical values $\tilde{\varepsilon}_c(N)$ computed for different numbers of sampling points (termination value $\Delta=2\times10^{-6}$) are

$2N$	64	128	256	512	1024
$\tilde{\varepsilon}_c$	0.01688	0.02312	0.02594	0.02750	0.02781

For $2N=512$ and $2N=1024$ the $\tilde{\varepsilon}_c(N)$ values that we find are are close to the threshold $\varepsilon_c\approx0.02759$ estimated in Ref. [55]. The invariant torus with $\varepsilon=0.02781$, $2N=1024$, and $\Delta=2\times10^{-6}$ shown in Fig. 5(a) exhibits a nonsmoothness and uneven distribution of discretization points characteristic of criticality. Setting $\Delta=10^{-6}$ leads to the invariant torus with the critical value estimate $\tilde{\varepsilon}_c=0.018\,44$, displayed in Fig. 5(b). It looks smooth, indicating that it is far from criticality and thus that the termination value is too small.

C. Two coupled standard maps

In principle, the Newton descent method is applicable to determination of invariant tori of arbitrary dimension for flows or maps of arbitrary dimension. In practice, one is severely limited by computational constraints.

In order to test the feasibility of the method in higher dimensions, here we consider two coupled standard maps [63]

$$\begin{aligned}
I_{n+1}&=I_n+\epsilon_1\sin\theta_n+\epsilon_3\sin(\theta_n+\psi_n),\\
\theta_{n+1}&=\theta_n+I_{n+1},\\
J_{n+1}&=J_n+\epsilon_2\sin\psi_n+\epsilon_3\sin(\theta_n+\psi_n),\\
\psi_{n+1}&=\psi_n+J_{n+1},
\end{aligned} \tag{22}$$

with four-dimensional phase space, and demonstrate that the method can determine one- and two-dimensional invariant tori. The fictitious time dynamics (15) acts on the $\mathbf{x}=(\theta_n,I_n,\Psi_n,J_n)$ phase space, with dynamics $\mathbf{f}(\mathbf{x})$ defined by Eqs. (22).

First, we apply the fixed shift (19) fictitious time dynamics to determination of the one-dimensional golden-mean invariant torus with shift $\omega=\omega_g$. For the initial guess torus we take the integrable case torus $\epsilon_1=\epsilon_2=\epsilon_3=0$:

$$\mathbf{x}(s)=(s,\omega_g,s,\omega_g). \tag{23}$$

In the numerical calculation we search for a typical 1D invariant torus, with (arbitrarily chosen) small coupling values $\epsilon_1=0.1$, $\epsilon_2=0.15$, and $\epsilon_3=0.005$.

The invariant torus obtained by the fictitious time dynamics in this case is shown in Fig. 6. Numerically, $\theta=\psi$, indicating that for this one-dimensional torus the two phases are

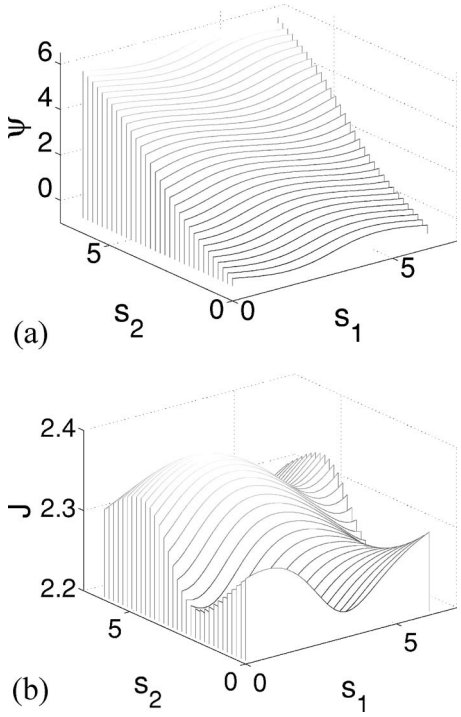

FIG. 7. The two-dimensional invariant torus of the coupled standard maps (22) with incommensurate frequencies $\omega_1=\omega_g$ and $\omega_2=\pi(\sqrt{3}-1)$ for $\epsilon_1=0.07$, $\epsilon_2=0.1$, and $\epsilon_3=0.004$. $(2N)^2=1024$ point discretization of the torus, termination value $\Delta=10^{-4}$.

entrained. The torus appears very smooth, indicating that for the parameter values chosen it is far from the critical values.

Next, we apply the Newton descent to the determination of a *two-dimensional* torus with nonresonant frequencies ω_1 and ω_2. In this case, we need two cyclic parameters $(s_1,s_2)\in[0,2\pi]^2$ to locate a point on the torus. The fictitious time evolution equation is similar to Eq. (19) but now we take

$$\mathbf{k}=\begin{pmatrix}k_1\\k_2\end{pmatrix},\quad \omega=\begin{pmatrix}\omega_1\\\omega_2\end{pmatrix},\quad \mathbf{s}=\begin{pmatrix}s_1\\0\\s_2\\0\end{pmatrix},\quad \mathbf{e}_1=\begin{pmatrix}1&0\\0&0\\0&1\\0&0\end{pmatrix}.$$

The initial guess is chosen as in the integrable $\epsilon_i=0$ case

$$\mathbf{x}(s_1,s_2)=(s_1,\omega_1,s_2,\omega_2). \tag{24}$$

In the numerical experiment we then search for (arbitrarily chosen) $\epsilon_1=0.07$, $\epsilon_2=0.1$, and $\epsilon_3=0.004$ two-dimensional invariant torus with (also arbitrarily chosen) frequencies $\omega_1=\omega_g$ and $\omega_2=\pi(\sqrt{3}-1)$. In order to reduce the computational time, we take a rather coarse $2N=32$ grid, with $(2N)^2=1024$ points representing the torus.

Two projections of the resulting invariant torus for $\Delta=10^{-4}$ termination value are shown in Fig. 7. While the $\psi(s_1,s_2)$ and $J(s_1,s_2)$ dependence on s_1 and s_2 shown in Fig. 7 follows in shape the integrable case (24) dependence, the small coupling terms induce significant oscillations. The smoothness of the invariant torus indicates that the parameters are not close to the critical values. For $(2N)^2=1024$ point discretization of the torus, Δ can be as low as 5.1×10^{-5} and for $(2N)^2=4096$ as low as 1.6×10^{-5}. However, the computation takes at least 100 times longer, and in this exploratory study the larger $(2N)^2$ resolutions were out of reach.

D. Kuramoto-Sivashinsky system

In our last example, we apply the Newton descent to the determination of an invariant two-torus embedded in a high-dimensional strongly contracting flow. Special tori that can be converted to periodic orbits in a rotating or moving frame have previously been computed for the complex Ginzburg-Landau equation [31] and for the 2D Poiseulle flow [56]. Here we shall determine a generic two-torus of the Kuramoto-Sivashinsky equation [57–59] parametrized by the system size L,

$$u_t=(u^2)_x-u_{xx}-u_{xxxx},\quad x\in[0,L]. \tag{25}$$

The Kuramoto-Sivashinsky equation describes the interfacial instabilities in a variety of contexts, like the flame front propagation [58], the two-fluid model [60] and the liquid film on an inclined plane [61].

In the study of flame fluttering on a gas ring as the system size L increases, the "flame front" becomes increasingly unstable and turbulent. As shown in Refs. [8,62], in dissipative systems two-dimensional tori often result from a Hopf bifurcation of a periodic orbit while three- (or higher-) dimensional tori are a rare occurrence. In the following we restrict our search to the antisymmetric solution space of Eq. (25) with periodic boundary conditions—i.e., $u(-x,t)=-u(x,t)$ and $u(x+L,t)=u(x,t)$, with $u(x,t)$ Fourier expanded as

$$u(x,t)=\sum_{k=-\infty}^{\infty} ia_k e^{ikqx}, \tag{26}$$

where $q=2\pi/L$ is the basic wave number and $a_{-k}=-a_k\in\mathbb{R}$. Accordingly, Eq. (25) becomes a set of ordinary differential equations

$$\dot{a}_k=[(kq)^2-(kq)^4]a_k-kq\sum_{m=-\infty}^{\infty} a_m a_{k-m}. \tag{27}$$

In the asymptotic regime of Eq. (27) for k large a_k's decay faster than exponentially, so a finite number of a_k's yields an accurate representation of the long-time dynamics. In our calculation, a truncation at $d=16$ suffices for a quantitatively accurate calculation.

In the current example, $2N=128$ points are used to represent the torus on the Poincaré section $a_1=0.06$. Numerical experimentation indicates that for $L=40.95$ trajectories spend significant fraction of time in a toroidal neighborhood, suggesting that a (partially hyperbolic?) invariant two-torus exists at this system size: Poincaré section returns of a typical orbit fall close to a closed curve. The initial guess for the Newton descent is constructed by choosing 128 more or less evenly distributed points to represent a guess loop on the Poincaré section and keeping the lower-wave-number modes of their Fourier transform. In this case the shift ω is fixed by

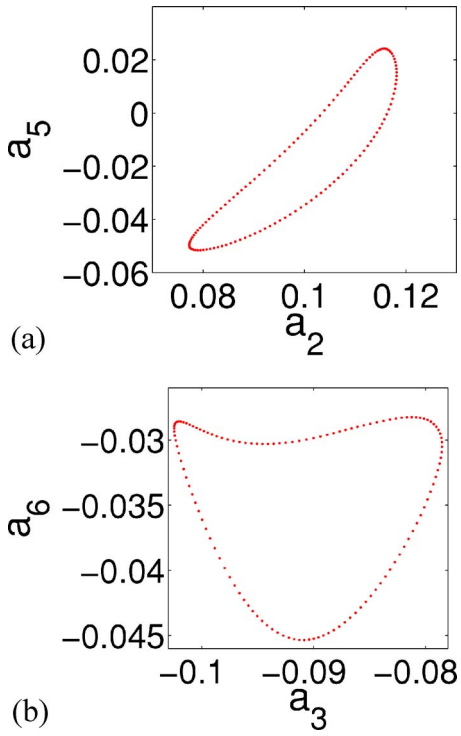

FIG. 8. (Color online) The projections of the two-dimensional invariant torus of Eq. (27) on the Poincaré section $a_1=0.06$ with shift $\omega=0.5968$ for $L=40.95$: Projection on (a) (a_2,a_5) and (b) (a_3,a_6). The Poincaré section return times are in the range $T=24.18\pm0.3$. $2N=128$ torus point parametrization, $\Delta=10^{-4}$ termination value.

the dynamics, and in order to compute it we impose the phase condition (12).

Figure 8 shows two Poincaré section projections, in the Fourier space, of the invariant two-torus of the Kuramoto-Sivashinsky flow determined by the Newton descent method. The method yields the shift $\omega=0.5968$. Even though the invariant torus is very smooth and discretization points are evenly distributed, surprisingly many sampling points are required to resolve the torus. For attempts with fewer discretization points—for example, $2N=64$—the search did not converge even with $\Delta=10^{-2}$.

V. SUMMARY

We have generalized the "Newton descent" method to determination of invariant m-tori in general d-dimensional dynamical systems and provided numerical evidence that the method converges in a large domain of existence of invariant tori, up to their breakups. In the case of maps and flows with invariant tori such as standard maps, the approach offers an alternative method for determining critical thresholds. While in principle the method is applicable to flows or maps in arbitrary dimension, computation can be expensive for invariant objects larger than one- and two-tori. We have utilized the smoothness of the fictitious time evolution to introduce acceleration schemes which improve the efficiency of the method.

In our numerical work, we have implemented the method in the constant shift (4) parametrization, Fourier representation of an m-torus $(m=1,2)$. Other discretizations could be better suited to specific applications. For instance, if an invariant torus is close to its critical threshold, representation of small fractal structures requires inclusion of slowly decaying high-wave-number Fourier modes, and so a large number of Fourier modes are needed to obtain an accurate representation. Furthermore, the discretization points distribute very nonuniformly when close to criticality which could considerably lower the accuracy of a representation. In this case, other nonconstant shift parametrizations of the torus dynamics might be more appropriate. For example, our method is of modest accuracy compared to some of current studies of critical tori, in particular Haro–de la Llave [11] computation of critical tori to 100 digits precision.

In periodic orbit searches we have found the Newton descent approach robust and very useful for finding periodic orbits in high-dimensional phase spaces where good guesses for multishooting Newton routines are hard to find [46,47]. Examples worked out here suggest that the method is also a robust starting point for m-dimensional invariant tori searches. Once an approximate invariant torus is found by the Newton descent method, it can be used as a starting guess for a high-precision method, such as some of the currently used Newton's methods in Fourier-space representations of invariant tori.

[1] P. Cvitanović, R. Artuso, R. Mainieri, G. Tanner, and G. Vattay, *Chaos: Classical and Quantum* (Niels Bohr Institute, Copenhagen, 2006).
[2] D. B. Wysham and J. D. Meiss, nlin.CD/0504054, and references therein.
[3] D. V. Treshev, Russ. J. Math. Phys. **2**, 93 (1994); S. V. Bolotin and D. V. Treshev, Regular Chaotic Dyn. **5**, 401 (2000); www.ma1.upc.es/intas/intas97/preprints97/i46bol_tre.ps
[4] M. W. Hirsch, C. C. Pugh, and M. Shub, *Invariant Manifolds, Lecture Notes in Mathematics*, Vol. 583 (Springer, New York, 1977).
[5] R. S. Mackay, J. D. Meiss, and I. C. Percival, Physica D **13**, 55 (1984).
[6] R. S. MacKay, J. D. Meiss, and I. C. Percival, Phys. Rev. Lett. **52**, 697 (1984).
[7] P. Cvitanović, *Universality in Chaos* (Adam Hilger, Bristol, 1989).
[8] S. E. Newhouse, D. Ruelle, and F. Takens, Commun. Math. Phys. **64**, 35 (1978).
[9] Q. Chen, J. D. Meiss, and I. C. Percival, Physica D **29**, 143 (1987).
[10] B. Mestel and I. Percival, Physica D **24**, 172 (1987).
[11] A. Haro and R. de la Llave, mp_arc#04-348; mp_arc#04-350; Chaos **16**, 013120 (2006); mp_arc#05-246.

[12] J. Laskar, in *Hamiltonian Systems with Three or More Degrees of Freedom*, edited by C. Simó (Kluwer Academic, Dordrecht, 1999).
[13] J. Laskar, C. Froeschlé, and A. Celletti, Physica D **56**, 253 (1992).
[14] J. H. E. Cartwright, M. O. Magnasco, and O. Piro, Phys. Rev. E **65**, 045203(R) (2002).
[15] A. Babiano, J. H. E. Cartwright, O. Piro, and A. Provenzale, Phys. Rev. Lett. **84**, 5764 (2000).
[16] J. Botina and H. Rabitz, Phys. Rev. Lett. **75**, 2948 (1995).
[17] J. M. Greene, J. Math. Phys. **20**, 1183 (1979).
[18] S. Tompaidis, Exp. Math. **5**, 211 (1995).
[19] R. S. MacKay, Nonlinearity **5**, 161 (1992).
[20] T. S. Parker and L. O. Chua, *Practical Numerical Algorithms for Chaotic Systems* (Springer, New York 1989).
[21] C. Simó, in *Les Méthodes Modernes de la Mécanique Céleste*, edited by D. Benest and C. Froeschlé (Editions Frontières, Paris, 1990), pp. 285–329. Available at http://www.dynamicalsystems.org/tu/
[22] I. G. Kevrekidis, R. Aris, L. D. Schmidt, and S. Pelikan, Physica D **16**, 243 (1985).
[23] L. Debraux, Contemp. Math. **172**, 169 (1994).
[24] G. Moore, SIAM (Soc. Ind. Appl. Math.) J. Numer. Anal. **33**, 2333 (1996).
[25] M. van Veldhuizen, SIAM (Soc. Ind. Appl. Math.) J. Sci. Stat. Comput. **8**, 951 (1987).
[26] H. W. Broer, H. M. Osinga, and G. Vegter, ZAMP **48**, 480 (1997).
[27] L. Dieci, J. Lorenz, and R. D. Russell, SIAM (Soc. Ind. Appl. Math.) J. Sci. Stat. Comput. **12**, 607 (1991).
[28] H. Mingyou, T. Küpper, and N. Masbaum, SIAM J. Sci. Comput. (USA) **18**, 918 (1997).
[29] T. Ge and A. Y. T. Leung, Nonlinear Dyn. **15**, 283 (1998).
[30] F. Schilder, H. M. Osinga, and W. Vogt, SIAM J. Appl. Dyn. Syst. **4**, 459 (2005).
[31] V. López, P. Boyland, M. T. Heath, and R. D. Moser, SIAM J. Appl. Dyn. Syst. **4**, 1042 (2005).
[32] R. L. Warnock and R. D. Ruth, Physica D **26**, 1 (1987).
[33] E. Castellà and À. Jorba, Celest. Mech. Dyn. Astron. **76**, 35 (2000).
[34] À. Jorba and M. Ollé, Nonlinearity **17**, 691 (2004).
[35] F. Schilder, W. Vogt, S. Schreiber, and H. M. Osinga (unpublished).
[36] M. Kaasalainen, Phys. Rev. E **52**, 1193 (1995).
[37] R. L. Warnock, Phys. Rev. Lett. **66**, 1803 (1991).
[38] I. C. Percival, J. Phys. A **7**, 794 (1974).
[39] I. C. Percival, J. Phys. A **12**, L57 (1979).
[40] H.-T. Kook and J. D. Meiss, Physica D **35**, 65 (1989).
[41] J. N. Mather, J. Am. Math. Soc. **4**, 207 (1991).
[42] W. E. Gabella, R. D. Ruth, and R. L. Warnock, Phys. Rev. A **46**, 3493 (1992).
[43] H. B. Keller, *Numerical Methods for Two-Point Boundary-Value Problems* (Dover, New York, 1992).
[44] J. Stoer and R. Bulirsch, *Introduction to Numerical Analysis* (Springer, New York, 1983).
[45] W. H. Press, S. A. Teukolsky, W. T. Vetterling, and B. P. Flannery, *Numerical Recipes in C* (Cambridge University Press, Cambridge, England, 1992).
[46] P. Cvitanovic and Y. Lan, in *Proceedings of the 10th International Workshop on Multiparticle Production: Correlations and Fluctuations in QCD*, edited by N. Antoniou (World Scientific, Singapore, 2003).
[47] Y. Lan and P. Cvitanovic, Phys. Rev. E **69**, 016217 (2004).
[48] L. Onsager and S. Machlup, Phys. Rev. **91**, 1505 (1953).
[49] M. Gromov, Invent. Math. **82**, 307 (1985).
[50] A. Floer, J. Diff. Geom. **28**, 513 (1988).
[51] V. I. Arnold, *Mathematical Methods for Classical Mechanics* (Spring, New York, 1989).
[52] J. M. Ball, Q. Appl. Math. **56**, 719 (1998).
[53] L. P. Kadanoff, Phys. Rev. Lett. **47**, 1641 (1981).
[54] S. J. Shenker and L. P. Kadanoff, J. Stat. Phys. **27**, 631 (1982).
[55] C. Chandre and H. R. Jauslin, Phys. Rep. **365**, 1 (2002).
[56] P. S. Casas and À. Jorba (unpublished).
[57] Y. Kuramoto, Suppl. Prog. Theor. Phys. **64**, 346 (1978).
[58] G. I. Sivashinsky, Acta Astronaut. **4**, 1177 (1977).
[59] P. Holmes, J. L. Lumley, and G. Berkooz, *Turbulence, Coherent Structures, Dynamical Systems and Symmetry* (Cambridge University Press, Cambridge, England, 1998).
[60] H.-C. Chang, Phys. Fluids **29**, 3142 (1986).
[61] H.-C. Chang, Annu. Rev. Fluid Mech. **26**, 103 (1994).
[62] D. Ruelle and F. Takens, Commun. Math. Phys. **20**, 167 (1971).
[63] K. Kaneko and R. J. Bagley, Phys. Lett. **110A**, 435 (1985).